Journal of Quantitative Spectroscopy & Radiative Transfer 118 (2013) 96–101

Contents lists available at SciVerse ScienceDirect

Journal of Quantitative Spectroscopy & Radiative Transfer

journal homepage: www.elsevier.com/locate/jqsrt

H_2O line positions in the 784–795 nm region with 10^{-9} accuracy

Y. Lu, X.-F. Li, J. Wang, A.-W. Liu, S.-M. Hu *

Hefei National Laboratory for Physical Sciences at Microscale, University of Science and Technology of China, Hefei 230026, China

ARTICLE INFO

Article history:
Received 28 September 2012
Received in revised form
14 November 2012
Accepted 20 November 2012
Available online 27 November 2012

Keywords:
Cavity ring-down
Water molecule
HITRAN

ABSTRACT

$H_2^{16}O$ lines in the spectral range of 12,573–12,753 cm^{-1} have been recorded by cavity ring-down spectroscopy. Low-pressure water vapor (0.25 Torr) was used to limit the pressure-induced line shift. The absolute line positions were calibrated with Rb atomic transitions and a thermo-stabilized Fabry–Pérot interferometer. Positions of 73 lines with intensities larger than 1×10^{-25} $cm^{-1}/(molecule\ cms^{-2})$ have been determined. For well-isolated lines, the absolute frequency accuracy is estimated to be 3×10^{-5} cm^{-1}, which is also confirmed by the ground-state combination differences. Comparison between the line positions obtained in this work and those from HITRAN shows a systematic deviation of 0.001 cm^{-1}.

1. Introduction

The ro-vibrational spectrum of water vapor has been of great interest for its importance in chemical, atmospheric and astronomical studies. Tremendous scientific efforts have been put into both experimental and theoretical studies. A huge archive of the transitions can be found in some widely used spectroscopic databases including HITRAN [1], GEISA [2], and HITEMP [3]. Very recently, a critical evaluation of the rotational–vibrational energy levels and transition frequencies of $H_2^{16}O$ has been carried out by Tennyson and co-workers [4]. Transitions of the water molecule are also widely used for spectral calibration for its extremely rich spectrum in the infrared. Most of the available infrared molecular absorption line frequencies were derived from Doppler-limited spectra and with typical accuracy of 10^{-4}–10^{-3} cm^{-1}.

To the best of our knowledge, the most precise water line positions were presented by Matsushima et al. [5] using a tunable far-infrared spectrometer. Line centers of the pure rotational transitions of $H_2^{16}O$ in the 0.5–5 THz region have been determined with an average accuracy of 100–200 kHz, or one part in 10^8. The hyperfine structures of $H_2^{16}O$ and $H_2^{18}O$ in the 0.18–0.56 THz region have been measured by Golubiatnikov et al. [6] using the Lamb-dip technique. Lisak and Hodges [7] measured the Lamb dips of a few blended H_2O lines near 7100 cm^{-1} with sub-MHz relative precision, but did not report the absolute transition frequencies.

In principle, an accurate line position can be retrieved from a broad line if the line profile has been recorded precisely, which requires a spectrometer with both high-sensitivity and high-resolution to detect small changes in the spectral profile. In this study, we present accurate frequency measurements of strong $H_2^{16}O$ lines in the 784–795 nm region. Most of these H_2O transitions belong to the $(\nu_2+3\nu_3)$ and $(\nu_1+\nu_2+2\nu_3)$ bands, which have been extensively studied before. Fourier-transform spectroscopy of water vapor absorption in this region has been reported first by Toth [8], and later by Flaud et al. [9], Schermaul et al. [10], and Mérienne et al. [11]. The estimated uncertainties of the transition frequencies were around 0.001–0.002 cm^{-1}. The line parameters and assignments [12] have been updated in the 2008 edition of HITRAN [1]. $H_2^{16}O$ transitions in this region have also been studied by intra-cavity laser absorption spectroscopy (ICLAS) [13–15] and cavity ring-down spectroscopy (CRDS) [16] with comparable frequency resolution but higher sensitivity.

Using a cavity ring-down spectrometer with a minimal detectable absorption coefficient of 1×10^{-10} cm^{-1}, we

* Corresponding author. Tel.: +86 551 63606557.
E-mail address: smhu@ustc.edu.cn (S.-M. Hu).

0022-4073/$ - see front matter © 2012 Elsevier Ltd. All rights reserved.
http://dx.doi.org/10.1016/j.jqsrt.2012.11.021

re-measure the doppler broadened spectra of 73 strongest $H_2^{16}O$ lines in the 12,573–12,753 cm^{-1} region. The absolute line frequencies are determined using a thermo-stabilized Fabry–Pérot interferometer (FPI) calibrated with precise atomic transitions. The estimated uncertainty of the obtained line positions is 3×10^{-5} cm^{-1}, or a few parts in 10^9. These $H_2^{16}O$ transition frequencies can be used as convenient optical frequency standards in this region.

2. Experimental

The details of the experimental setup have been presented in Refs. [17,18] and will be only briefly described here. A continuous-wave tunable Ti:sapphire laser (Coherent 899-21) beam is coupled into a 1.4 m long ring-down cavity. The cavity mirrors have a reflectivity of 99.995% and one of them is mounted on a piezoelectric actuator. The piezoelectric actuator is driven with a triangle wave from a function generator to repeatedly match the longitudinal mode of the ring-down cavity to the laser wavelength. The Ti:sapphire laser is run in a step-scan mode. At each step, typically about 100 ring-down events are recorded. The decay time τ is retrieved from a fit of the exponential decay curve. The sample absorption coefficient can be determined from [19]

$$\alpha=\frac{1}{c\tau}-\frac{1}{c\tau_0}, \tag{1}$$

where c is the speed of light, and τ_0 is the ring-down time of an empty cell.

Precise frequency calibration is accomplished by using the longitudinal modes of a 10 cm long thermo-stabilized Fabry–Pérot interferometer (FPI) made of ultra-low-expansion (ULE) glass and installed in a vacuum chamber. The finesse of the ULE-FPI is around 2000–5000 near 0.79 μm. Using the precise atomic transitions of ^{87}Rb at 795 nm [20] and 780 nm [21], the absolute frequencies of the longitudinal modes of the ULE-FPI in the region of 780–795 nm have been determined to be

$$\nu_N=\nu_{Rb}+\Delta_0+N\bar{f}, \tag{2}$$

where ν_{Rb} is the ^{87}Rb ($5S_{1/2}\rightarrow5P_{3/2}$, $F=2\rightarrow3$) transition frequency, 384 228 115.203(8) MHz from Ref. [21], $\Delta_0=389.213(63)$ MHz is the measured frequency shift of a nearby ULE-FPI peak relative to the Rb transition, N is the index of a ULE-FPI peak, and $\bar{f}=1497.02922(2)$ MHz is the determined free-spectral-range (FSR) in this region. As discussed in Ref. [18], the uncertainty of the ν_N values is estimated to be 0.1–0.6 MHz, possibly caused by the

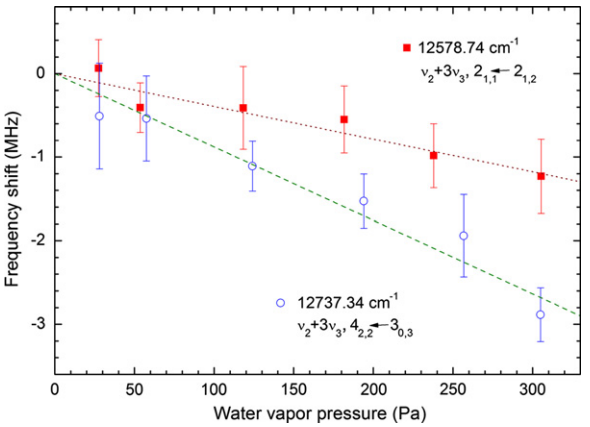

Fig. 2. Relative line centers derived from the spectra recorded with different water sample pressures. Solid squares: the $(\nu_2+3\nu_3)$ band $2_{1,1}\leftarrow2_{1,2}$ line at 12,578.74 cm^{-1}. Open circles: the $(\nu_2+3\nu_3)$ band $4_{2,2}\leftarrow3_{0,3}$ line at 12,737.34 cm^{-1}.

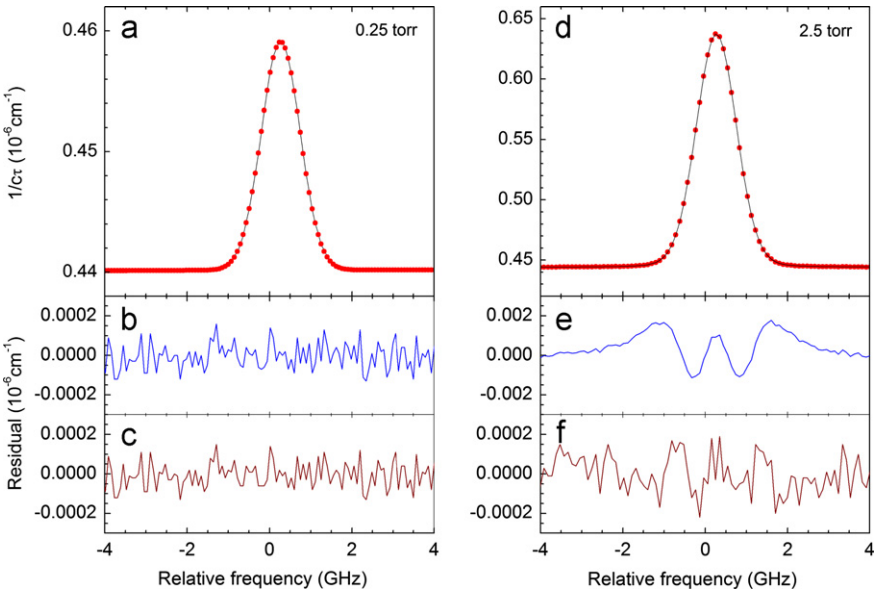

Fig. 1. Spectral fit of the H_2O line at 12737.344 cm^{-1}. (a) Recorded spectrum with 0.25 Torr (33 Pa) water vapor. (b) Residuals of the fit using a pure Gaussian profile. (c) Residuals using a Voigt profile. (d), (e), (f) are respectively the spectrum and the fitting residuals using Gaussian and Voigt profiles, water vapor pressure at 2.5 Torr.

Table 1
$H_2^{16}O$ line positions and upper level energies obtained in this work (in cm^{-1}).

V	Transition	v, this work	Δv[a]	S[b]	E_{up}	δE[c]
(1 1 2)	$4_{3,2}$–$3_{2,1}$	12,573.299621(22)	1679	6.41	12,785.455948	1049
(0 1 3)	$4_{2,2}$–$4_{2,3}$	12,573.742907[d]	893	5.41	12,874.105144	459
(0 1 3)	$2_{1,1}$–$2_{1,2}$	12,578.739573(15)	527	9.52	12,658.235943	729
(1 1 2)	$4_{3,1}$–$3_{2,2}$	12,580.299839(18)	1061	1.93	12,786.601238	1178
(1 1 2)	$5_{3,3}$–$4_{2,2}$	12,586.668631[d]	1269	1.12	12,902.448120	−1043
(0 1 3)	$1_{0,1}$–$0_{0,0}$	12,588.154719(20)	1181	6.09	12,588.154719	945
(0 1 3)	$3_{1,2}$–$3_{1,3}$	12,592.639362(22)	1138	1.51	12,734.917827	367
(1 1 2)	$6_{3,4}$–$5_{2,3}$	12,595.836809(31)	1291	1.49	13,042.347409	1801
(0 1 3)	$2_{1,2}$–$1_{1,1}$	12,604.066295(30)	1205	7.72	12,641.203414	1127
(1 1 2)	$5_{3,2}$–$4_{2,3}$	12,606.962052(19)	1648	2.36	12,907.324289	910
(1 1 2)	$4_{4,1}$–$3_{3,0}$	12,607.900075[d]	1425	6.49	12,893.318600	1095
(1 1 2)	$4_{4,0}$–$3_{3,1}$	12,608.099054(24)	846	2.17	12,893.318358	1289
(0 1 3)	$2_{0,2}$–$1_{0,1}$	12,609.071607(20)	1193	31.9	12,632.865957	630
(0 1 3)	$4_{1,3}$–$4_{1,4}$	12,609.636683[d]	1917	2.21	12,834.475030	462
(0 1 3)	$2_{1,1}$–$1_{1,0}$	12,615.864314(18)	1386	21.8	12,658.236041	631
(0 1 3)	$3_{1,3}$–$2_{1,2}$	12,621.736505(23)	1195	33.9	12,701.232875	712
(0 1 3)	$3_{0,3}$–$2_{0,2}$	12,626.644706(21)	1094	12.2	12,696.735509	868
(1 1 2)	$5_{4,2}$–$4_{3,1}$	12,626.937263(18)	2337	1.03	13,010.779722	1366
(0 1 3)	$3_{2,2}$–$3_{0,3}$	12,627.897554(41)	2246	1.19	12,764.659187	1008
(1 1 2)	$5_{4,1}$–$4_{3,2}$	12,628.320486(19)	1714	2.86	13,010.837313	2134
(0 1 3)	$3_{2,2}$–$2_{2,1}$	12,629.757599(19)	1001	16.0	12,764.659212	983
(0 1 3)	$3_{2,1}$–$2_{2,0}$	12,635.544696(31)	904	5.00	12,771.708596	1016
(0 1 3)	$4_{1,4}$–$3_{1,3}$	12,637.654340(23)	660	11.5	12,779.932805	74
(0 1 3)	$3_{1,2}$–$2_{1,1}$	12,639.741994(29)	1006	9.59	12,734.917918	276
(0 1 3)	$4_{0,4}$–$3_{0,3}$	12,640.738294(15)	906	33.5	12,777.499927	570
(1 1 2)	$6_{4,3}$–$5_{3,2}$	12,643.242245(23)	1955	1.34	13,152.054223	2839
(1 1 2)	$4_{3,2}$–$3_{0,3}$	12,648.694454[d]	1546	2.44	12,785.456087	910
(0 1 3)	$4_{2,3}$–$3_{2,2}$	12,649.702947(20)	353	6.63	12,856.004346	513
(0 1 3)	$4_{3,2}$–$3_{3,1}$	12,650.154069(13)	831	2.84	12,935.373373	867
(0 1 3)	$4_{3,1}$–$3_{3,0}$	12,651.768553(23)	1147	8.14	12,937.187078	1141
(0 1 3)	$5_{1,5}$–$4_{1,4}$	12,651.928839(28)	1161	30.5	12,876.767186	551
(0 1 3)	$5_{0,5}$–$4_{0,4}$	12,653.473295(17)	1205	9.82	12,875.526025	1073
(0 1 3)	$4_{1,3}$–$3_{1,2}$	12,661.108890(13)	1010	27.5	12,834.474668	825
(0 1 3)	$4_{2,2}$–$3_{2,1}$	12,661.948894(23)	806	19.3	12,874.105221	382
(0 1 3)	$6_{1,6}$–$5_{1,5}$	12,663.002588(20)	612	5.11	12,989.628011	1296
(0 1 3)	$6_{0,6}$–$5_{0,5}$	12,665.158444[d]	1356	22.5	12,990.506297	746
(0 1 3)	$5_{2,4}$–$4_{2,3}$	12,667.750327(12)	1073	17.7	12,968.112564	806
(0 1 3)	$5_{4,2}$–$4_{4,1}$	12,668.959874(17)	826	5.17	13,157.067493	1440
(0 1 3)	$5_{4,1}$–$4_{4,0}$	12,669.206973(24)	527	1.74	13,157.341070	1108
(1 1 2)	$6_{2,4}$–$5_{1,5}$	12,670.126497(23)	303	2.47	12,996.751920	520
(0 1 3)	$5_{3,3}$–$4_{3,2}$	12,671.861343(26)	357	9.47	13,054.378170	821
(0 1 3)	$7_{1,7}$–$6_{1,6}$	12,675.430045(21)	1155	14.3	13,122.682324	1330
(0 1 3)	$7_{0,7}$–$6_{0,6}$	12,675.942744(15)	1456	4.90	13,122.639272	939
(0 1 3)	$5_{3,2}$–$4_{3,1}$	12,676.899412(22)	1088	3.06	13,060.741871	1804
(0 1 3)	$5_{1,4}$–$4_{1,3}$	12,678.808619(20)	1981	6.87	12,954.305622	433
(0 1 3)	$6_{2,5}$–$5_{2,4}$	12,683.780339(19)	1261	4.11	13,099.989022	1393
(0 1 3)	$8_{1,8}$–$7_{1,7}$	12,685.537678(30)	722	2.87	13,272.016780	172
(0 1 3)	$8_{0,8}$–$7_{0,7}$	12,685.767947(29)	1053	8.42	13,272.011401	−43
(0 1 3)	$5_{2,3}$–$4_{2,2}$	12,687.066076(22)	124	5.19	13,002.845565	−789
(0 1 3)	$6_{4,3}$–$5_{4,2}$	12,692.160723[d]	1977	1.59	13,302.275070	613
(0 1 3)	$6_{3,4}$–$5_{3,3}$	12,692.189699[d]	601	2.28	13,196.157733	−1600
(0 1 3)	$6_{1,5}$–$5_{1,4}$	12692.408510(27)	1190	13.2	13,091.865963	365
(0 1 3)	$6_{4,2}$–$5_{4,1}$	12,693.133956(22)	1144	4.21	13,303.475030	410
(0 1 3)	$9_{1,9}$–$8_{1,8}$	12,694.408505(20)	495	4.55	13,438.571059	1030
(0 1 3)	$9_{0,9}$–$8_{0,8}$	12,694.495215(16)	885	1.56	13,438.558772	−843
(0 1 3)	$7_{2,6}$–$6_{2,5}$	12,698.490391(20)	709	7.82	13,251.401698	631
(0 1 3)	$10_{0,10}$–$9_{0,9}$	12,702.198399[d]	601	2.19	13,622.366607	−617
(0 1 3)	$7_{1,6}$–$6_{1,5}$	12,702.954940(19)	1560	2.50	13,245.860644	653
(0 1 3)	$6_{3,3}$–$5_{3,2}$	12,703.098852(19)	548	6.63	13,211.910830	851
(1 1 2)	$6_{6,1}$–$5_{5,0}$	12,708.345241(31)	259	2.02	13,450.421468	−1145
(0 1 3)	$6_{2,4}$–$5_{2,3}$	12,709.352360(20)	740	9.82	13,155.862960	882
(0 1 3)	$7_{3,5}$–$6_{3,4}$	12,709.948000(26)	1400	2.90	13,358.926589	217
(3 1 0)	$7_{6,1}$–$6_{3,4}$	12,711.888393(12)	2307	1.58	13,360.866982	1274
(0 1 3)	$8_{1,7}$–$7_{1,6}$	12,712.010871(20)	929	4.04	13,416.224815	−374
(0 1 3)	$7_{4,4}$–$6_{4,3}$	12,714.019106(12)	−6	2.60	13,470.743770	−779
(0 1 3)	$9_{2,8}$–$8_{2,7}$	12,717.953034(19)	1066	1.85	13,603.553109	1067
(0 1 3)	$7_{2,5}$–$6_{2,4}$	12,727.708863(22)	1337	1.91	13,330.482273	974
(0 1 3)	$7_{3,4}$–$6_{3,3}$	12,728.870538(23)	−338	1.22	13,390.419361	430
(1 1 2)	$7_{6,1}$–$6_{5,2}$	12,729.619965(24)	135	1.17	13,618.218572	846

Table 1 (*continued*)

V	Transition	ν, this work	$\Delta\nu$[a]	S[b]	E_{up}	δE[c]
(0 1 3)	$4_{2,\,2}$–$3_{0,\,3}$	12,737.343579(22)	821	1.09	12874.105212	391
(0 1 3)	$8_{4,\,4}$–$7_{4,\,3}$	12,741.012423(24)	877	1.21	13,672.249386	964
(0 1 3)	$8_{2,\,6}$–$7_{2,\,5}$	12,741.393452(21)	2048	2.61	13,523.803160	−2273
(0 1 3)	$8_{3,\,5}$–$7_{3,\,4}$	12,752.161924(23)	−224	1.79	13,594.518388	−92

[a] $\delta\nu = \nu_{HITRAN} - \nu_{this}$, in 10^{-6} cm^{-1}.
[b] Line strength (in 10^{-25} cm/molecule) from HITRAN [1].
[c] $\delta E = E_{MARVEL} - E_{this}$ in 10^{-6} cm^{-1}, E_{MARVEL} is upper level energy from Ref. [4].
[d] Blended lines.

variation of the FSR due to the group-delay-dispersion of the ULE-FPI mirrors. The spectrometer has been applied to determine the absolute frequency of the $S_3(3)$ line ($V = 3 \leftarrow 0$, $J = 5 \leftarrow 3$) of H_2 at 796 nm with an accuracy of 1.6 MHz [22].

A sample of distilled water was used without further purification. Water vapor pressures were measured with a capacitance manometer with a stated relative uncertainty of 0.12%. Spectra of 73 water lines in the 784–795 nm region with line strengths larger than 1×10^{-25} cm^{-1}/(molecule cm^{-2}) were recorded at room temperature (296 K). For each line, the spectrum was typically recorded 5–8 times under the same experimental conditions.

3. Results and discussion

3.1. Determination of the line positions

The water line positions are determined from the spectra recorded with a sample pressure of 0.25 torr (33 Pa). Using a least-squares fit of the spectral profile, the relative frequency shift of the line center to a nearby ULE-FPI peak is derived, and the absolute line frequency is determined by adding the frequency shift to the ULE-FPI peak frequency ν_N given in Eq. (2). For each line, the absorption profile is measured several times and the averaged line center and respective statistical deviation are derived from fits of the spectra.

As an example, the spectrum of the $H_2^{16}O$ line at 12,737.344 cm^{-1} is presented in Fig. 1. For the spectrum recorded at such a low sample pressure of 33 Pa, the pressure-induced effects are negligible: as is illustrated in Fig. 1(b) and (c), the spectral profile can be almost equally well reproduced by either a pure Gaussian function or a Voigt function. Pressure-induced effects including the self-pressure shift and broadening can be observed at higher water sample pressures. Fig. 1(d) shows the spectrum of the same line recorded at 2.5 torr (330 Pa). The line profile cannot be well reproduced by a Gaussian function (Fig. 1(e)) but can be well reproduced by a Voigt function, which has residuals (Fig. 1(f)) at the noise level.

The pressure-induced line shift is also detectable. Fig. 2 shows the relative frequency shifts of the lines at 12,578.74 and 12,737.34 cm^{-1} measured at different sample pressures. The coefficients, δ_{self}, derived for these two lines, are −0.013(2) cm^{-1} atm^{-1} and −0.029(3) cm^{-1} atm^{-1}, respectively. The self-pressure-induced line shift coefficients in this region have not been reported before. As a point of

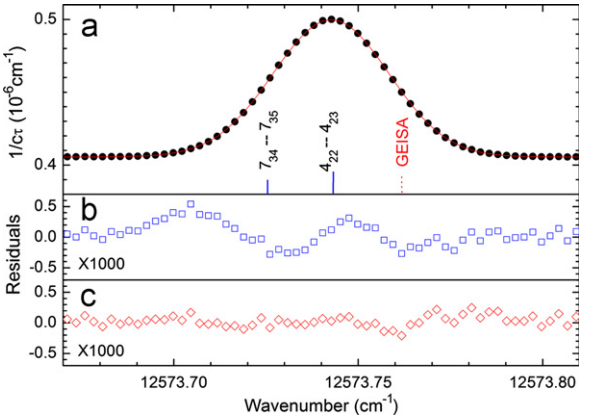

Fig. 3. Spectral fit of the $H_2^{16}O$ lines around 12,573.743 cm^{-1}. (a) CRDS experimental spectrum. The GEISA position of the $7_{3,4} \leftarrow 7_{3,5}$ line is 0.04 cm^{-1} larger than the value calculated in this work. (b) Residuals of the fit when only one line is included. Both line position and intensity are fitted. (c) Residuals of the fit when two lines are included. The weak $7_{3,4} \leftarrow 7_{3,5}$ line position was fixed at the calculated value in the fit (see main text).

comparison, most of the air pressure-induced line shift, δ_{air}, values given in HITRAN are set to 0 or to the default value of −0.0111 cm^{-1} atm^{-1}. The line-by-line pressure-induced shift studies will not be presented here. At a water vapor pressure of 0.25 Torr, the pressure-induced position shift should be well below 1×10^{-5} cm^{-1}. It is therefore neglected in this study as it is less than the experimental uncertainty.

Owing to the high signal-to-noise ratio achieved in the CRDS measurements, the center of the observed water lines can be determined with an uncertainty of 3×10^{-5} cm^{-1}, which is only 0.1% of the Doppler width (FWHM 0.037 cm^{-1}, or 1.1 GHz). The positions of 73 transitions with intensities larger than 1×10^{-25} cm^{-1}/(molecule cm^{-2}) are obtained in this work and are given in Table 1. The list contains 58 lines reaching the (013) vibrational state, 14 lines reaching the (112) state and 1 line reaching the (310) state. All transitions are from the (000) ground vibrational state. For comparison, the assignments, positions and strengths from HITRAN (originally from Ref. [12]) are also given in the table.

3.2. The overlapping lines

It is worth noting that line overlapping can introduce a systematic shift on the determined line centers, which

can be much larger than the statistical uncertainty given in Table 1. According to the fit of the observed spectrum and the line list given in the HITRAN database, nine lines marked with "*" in Table 1 are confirmed to be blended lines. The centers of these lines have been derived using multi-peak fits. Due to limited knowledge of the overlapping counterpart (weaker water lines) and the correlations among the parameters used in the fits, errors on the derived centers of the overlapping lines may be as large as 0.0005 cm^{-1}, over 10 times larger than the statistical uncertainty. The situation may be better when the position of the overlapping weak line can be determined elsewhere and fixed in the multi-peak fitting.

Fig. 3(a) shows the recorded spectrum of the line near 12,573.74 cm^{-1}. In HITRAN [1] (and in Ref. [12]), this line was assigned as the $4_{2,2} \leftarrow 4_{2,3}$ transition of the (013) band of $H_2^{16}O$, with a position of 12,573.7438 cm^{-1} and an intensity of 5.41×10^{-25} cm^{-1}/(molecule cm^{-2}). However, the spectrum cannot be fit well if only one peak is included in the fit. The residuals of the fit shown in Fig. 3(b) are much larger than the experimental uncertainty. In the GEISA database [2], beside the (013) $4_{2,2} \leftarrow 4_{2,3}$ line, a weaker line, 12,573.7656 cm^{-1}, 1.705×10^{-26} cm^{-1}/(molecule cm^{-2}), is given and assigned as (013) $7_{3,4} \leftarrow 7_{3,5}$. Using the (013) $7_{3,4} \leftarrow 6_{3,3}$ line position determined in this work and the respective lower level energies given in Ref. [23], the (013) $7_{3,4} \leftarrow 7_{3,5}$ transition frequency can be precisely predicted to be 12,573.725237 cm^{-1}. Note that the value has a −0.04 cm^{-1} difference from that given in GEISA. This difference is indicated in Fig. 3(a). The experimental spectrum was fit again with two lines included in the fitting, with the $7_{3,4} \leftarrow 7_{3,5}$ line position being fixed at the predicted value given above. The residuals of the fit are shown in Fig. 3(c). The obtained $4_{2,2} \leftarrow 4_{2,3}$ line position is 12, 573.742907 cm^{-1}. As will be discussed in Section 3.3, the obtained line frequency agrees very well with other transitions to the common upper level.

The situation is similar for the $(v_1+v_2+2v_3)$ $5_{3,3} \leftarrow 4_{2,2}$ line at 12,586.67 cm^{-1}. The line overlaps with the $5_{2,3} \leftarrow 5_{2,4}$ transition of the (v_2+3v_3) band. Since the $5_{2,3}$ (013) level energy can be derived using the transition at 12,687.066076 cm^{-1} presented in Table 1, the $5_{2,3} \leftarrow 5_{2,4}$ (013) line frequency can be predicted to be 12, 586.636882 cm^{-1}. With the weak line frequency fixed at this value, the position of the (112) $5_{3,3} \leftarrow 4_{2,2}$ line can be derived from the fit with better confidence.

3.3. Comparison with literature values

Using the rotational energies given by Furtenbacher and Császár [23], precise upper level energies can be derived using the transition frequencies obtained in this work. The obtained upper level energies are given in Table 1. There are several pairs of transitions with common upper levels and they are collected in Table 2. The combination differences can be used as a good indicator of the experimental uncertainty of the present study. As can be seen from Table 2, for isolated lines, the combination differences agree well with the experimental uncertainty. For the blended lines, the deviations are about one order of magnitude larger. In general, a large deviation often indicates improperly modeled or undiscovered overlapping on the line.

As the strongest water lines in this spectral range, the lines studied here have been reported in literatures [8–16]. In the HITRAN 2008 edition, the positions and intensities of these line are originally from the work by Tolchenov and Tennyson [12]. The accuracy of these lines stated in HITRAN was 0.0001−0.001 cm^{-1}. Fig. 4 shows the differences between the line positions given here and those given in HITRAN. A systematic deviation can be readily seen from the figure. The averaged deviation is 1.05×10^{-3} cm^{-1}. The deviation gradually increases when the line intensity decreases, which may be a result of insufficient sensitivity in previous studies.

A huge database of the ro-vibrational energies has been recently available from a MARVEL analysis of all available experimental transitions of $H_2^{16}O$ [4]. The differences between the energies from Ref. [4] and this work are given in the last column of Table 1. Note that the MARVEL energies of these levels are mainly determined

Table 2
Upper level energy determined with transitions to common upper level but from different lower levels (in cm^{-1}).

V, J	E'	Δ[a]	J''	E''[b]	ν
(013) $2_{1,1}$	12,658.235992	49	$1_{1,0}$	42.371726_6	12,615.864314 (18)
		−49	$2_{1,2}$	79.496369_9	12,578.739573 (15)
(013) $3_{1,2}$	12,734.917873	45	$2_{1,1}$	95.175924_3	12,639.741994 (29)
		−45	$3_{1,3}$	142.278465_4	12,592.639362 (22)
(013) $3_{2,2}$	12,764.659199	12	$2_{2,1}$	134.901612_7	12,629.757599 (19)
		−12	$3_{0,3}$	136.761633_0	12,627.897554 (41)
(112) $4_{3,2}$	12,785.455948	139	$3_{0,3}$	136.761633_0	12,648.694454[c]
		0	$3_{2,1}$	212.156327_2	12,573.299621 (22)
(013) $4_{1,3}$	12,834.474668	0	$3_{1,2}$	173.365777_5	12,661.108890 (13)
		363	$4_{1,4}$	224.838347_1	12,609.636683[c]
(013) $4_{2,2}$	12,874.105217	−5	$3_{0,3}$	136.761633_0	12,737.343579 (22)
		5	$3_{2,1}$	212.156327_2	12,661.948894 (23)
		−73	$4_{2,3}$	300.362236_6	12,573.742907[c]

[a] Combination difference, in 10^{-6} cm^{-1}.
[b] Lower level energies from Ref. [23].
[c] Blended lines which may have deviations as large as 0.0005 cm^{-1}, not included in the determination of upper level energies.

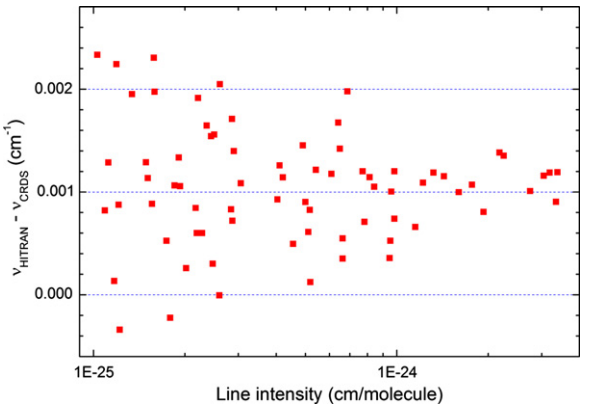

Fig. 4. Differences in the water line positions between HITRAN and this work.

from the transitions given in Ref. [12], and a calibration factor of 0.999 999 89(3) was applied to that experimental data source [4]. The averaged deviation of the upper energy levels has been reduced to 0.624×10^{-3} cm^{-1}, while the maximum reaches about 0.003 cm^{-1}.

4. Conclusion

In total, 73 H_2^{16} O absorption lines in the 784–795 nm region with cut-off line intensity of 1×10^{-25} cm^{-1}/(molecule cm^{-2}) have been studied using cavity ring-down spectroscopy. Except for some overlapping lines, the absolute positions of most well-isolated lines are determined to 3×10^{-5} cm^{-1} accuracy using the ^{87}Rb atomic line references at 780 nm and 795 nm. Compared with the results determined in this work, the line positions given in the HITRAN database have an averaged shift of 0.001 cm^{-1}, and the upper level energies given in recent MARVEL analysis have an averaged shift of 0.0006 cm^{-1}. We hope the line list provided here can be used as a convenient frequency standard in this spectral range.

Acknowledgments

This work is jointly supported by NSFC (21225314, 90921006, 20903085), NBRPC (2013CB834602) and FRFCU.

References

[1] Rothman L, Gordon I, Barbe A, Benner DC, Bernath P, Birk M, et al. The hitran 2008 molecular spectroscopic database. J Quant Spectrosc Radiat Transfer 2009;110:533–72.
[2] Jacquinet-Husson N, Crepeau L, Armante R, Boutammine C, Chedin A, Scott NA, et al. The 2009 edition of the GEISA spectroscopic database. J Quant Spectrosc Radiat Transfer 2011;112:2395–445.
[3] Rothman LS, Gordon IE, Barber RJ, Dothe H, Gamache RR, Goldman A, et al. HITEMP, the high-temperature molecular spectroscopic database. J Quant Spectrosc Radiat Transfer 2010;111:2139–50.
[4] Tennyson J, Bernath PF, Brown LR, Campargue A, Császár AG, Daumont L, et al. IUPAC critical evaluation of the rotational-vibrational spectra of water vapor. Part III: energy levels and transition wavenumbers for $H_2^{16}O$. J Quant Spectrosc Radiat Transfer; 2012 〈http://dx.doi.org/10.1016/j.jqsrt2012.10.002〉.
[5] Matsushima F, Odashima H, Iwasaki T, Tsunekawa S, Takagi K. Frequency-measurement of pure rotational transitions of H_2O from 0.5 to 5 THz. J Mol Struct 1995;352:371–8.
[6] Golubiatnikov GY, Markov VN, Guarnieri A, Knochel R. Hyperfine structure of $H_2^{16}O$ and $H_2^{18}O$ measured by Lamb-dip technique in the 180–560 GHz frequency range. J Mol Spectrosc 2006;240:251–4.
[7] Lisak D, Hodges JT. High-resolution cavity ring-down spectroscopy measurements of blended H_2O transitions. Appl Phys B 2007;88:317–25.
[8] Toth RA. Measurements of $H_2^{16}O$ line positions and strengths −11610 to 12861 cm^{-1}. J Mol Spectrosc 1994;166:176–83.
[9] Flaud JM, Camy-Peyret C, Bykov A, Naumenko O, Petrova T, Scherbakov A, et al. The high-resolution spectrum of water vapor between 11 600 and 12 750 cm^{-1}. J Mol Spectrosc 1997;183:300–9.
[10] Schermaul R, Learner RCM, Newnham DA, Williams RG, Ballard J, Zobov NF, et al. The water vapor spectrum in the region 8600−15 000 cm^{-1}: experimental and theoretical studies for a new spectral line database. I. Laboratory measurements. J Mol Spectrosc 2001;208:32–42.
[11] Mérienne MF, Jenouvrier A, Hermans C, Vandaele AC, Carleer M, Clerbaux C, et al. Water vapor line parameters in the 13 000−9250 cm^{-1} region. J Quant Spectrosc Radiat Transfer 2003;82:99–117.
[12] Tolchenov R, Tennyson J. Water line parameters from refitted spectra constrained by empirical upper state levels: study of the 9500−14 500 cm^{-1} region. J Quant Spectrosc Radiat Transfer 2008;109:559–68.
[13] Kalmar B, O'Brien JJ. Quantitative intracavity laser spectroscopy measurements with a Ti:sapphire laser: absorption intensities for water vapor lines in the 790–800 nm region. J Mol Spectrosc 1998;192:386–93.
[14] Mazzotti F, Naumenko OV, Kassi S, Bykov AD, Campargue A. ICLAS of weak transitions of water between 11 300 and 12 850 cm^{-1}: comparison with FTS databases. J Mol Spectrosc 2006;239:174–81.
[15] Campargue A, Mikhailenko S, Liu AW. ICLAS of water in the 770 nm transparency window (12 746–13 558 cm^{-1}). Comparison with current experimental and calculated databases. J Quant Spectrosc Radiat Transfer 2008;109:2832–45.
[16] Kassi S, Macko P, Naumenko O, Campargue A. The absorption spectrum of water near 750 nm by cw-CRDS: contribution to the search of water dimer absorption. Phys Chem Chem Phys 2005;7:2460–7.
[17] Gao B, Jiang W, Liu AW, Lu Y, Cheng CF, Cheng GS, et al. Ultra sensitive near-infrared cavity ring down spectrometer for precise line profile measurement. Rev Sci Instrum 2010;81:043105.
[18] Cheng CF, Sun YR, Pan H, Lu Y, Li XF, Wang J, et al. Cavity ring-down spectroscopy of Doppler-broadened absorption line with sub-MHz absolute frequency accuracy. Opt Express 2012;20:9956–63.
[19] Zalicki P, Zare RN. Cavity ring-down spectroscopy for quantitative absorption measurements. J Chem Phys 1997;102:2708–17.
[20] Maric M, McFerran JJ, Luiten AN. Frequency-comb spectroscopy of the D_1 line in laser-cooled rubidium. Phys Rev A 2008;77:032502.
[21] Ye J, Swartz S, Jungner P, Hall JL. Hyperfine structure and absolute frequency of the ^{87}Rb $5P_{3/2}$ state. Opt Lett 1996;21:1280–2.
[22] Cheng CF, Sun YR, Pan H, Wang J, Liu AW, Campargue A, et al. Electric-quadrupole transition of H_2 determined to 10^{-9} precision. Phys Rev A 2012;85:024501.
[23] Furtenbacher T, Császár AG. On employing $H_2^{16}O$, $H_2^{17}O$, $H_2^{18}O$, and $D_2^{16}O$ lines as frequency standards in the 15−170 cm^{-1} window. J Quant Spectrosc Radiat Transfer 2008;109:1234–51.